AIP | The Journal of Chemical Physics

A comprehensive study of the vibrationally resolved S 2p 1 Auger electron spectrum of carbonyl sulfide

V. Sekushin, R. Püttner, R. F. Fink, M. Martins, Y. H. Jiang, H. Aksela, S. Aksela, and G. Kaindl

Citation: The Journal of Chemical Physics **137**, 044310 (2012); doi: 10.1063/1.4734310
View online: http://dx.doi.org/10.1063/1.4734310
View Table of Contents: http://scitation.aip.org/content/aip/journal/jcp/137/4?ver=pdfcov
Published by the AIP Publishing

A comprehensive study of the vibrationally resolved S $2p^{-1}$ Auger electron spectrum of carbonyl sulfide

V. Sekushin,[1] R. Püttner,[1] R. F. Fink,[2,a)] M. Martins,[1,b)] Y. H. Jiang,[1,c)] H. Aksela,[3] S. Aksela,[3] and G. Kaindl[1]

[1]*Institut für Experimentalphysik, Freie Universität Berlin, Arnimallee 14, D-14195 Berlin-Dahlem, Germany*
[2]*Institute of Physical and Theoretical Chemistry, University of Würzburg, Am Hubland, D-97074 Würzburg, Germany*
[3]*University of Oulu, Department of Physics, P.O. Box 3000, 90401 Oulu, Finland*

(Received 20 March 2012; accepted 24 June 2012; published online 27 July 2012)

High-resolution normal Auger-electron spectra of carbonyl sulfide subsequent to S $2p^{-1}$ photoionization at photon energies of 200, 220, and 240 eV are reported along with corresponding photoelectron spectra. In addition, theoretical results are presented that take the core-hole orientation of the various spin-orbit-split and molecular-field-split S $2p^{-1}$ states into account. Auger transitions to eight metastable dicationic final states are observed and assigned on the basis of the theoretical results. From Franck-Condon analysis, assuming Morse potentials along the normal coordinates for seven of the observed quasi-stable dicationic final states, information on the potential-energy surfaces is derived and compared with theoretical results from the literature. © *2012 American Institute of Physics*. [http://dx.doi.org/10.1063/1.4734310]

I. INTRODUCTION

Carbonyl sulfide (OCS) is the major sulfur compound naturally present in the earth's atmosphere and it is emitted from the oceans or by volcanos. It plays a role in the formation of aerosols in the atmosphere and has, therefore, influence on the earth's climate. In addition, L. Leman and co-workers have demonstrated that in prebiotic chemistry OCS plays a role in the formation of peptides from amino acids,[1] i.e., it may be an important molecule in the formation of proteins and hence for the development of life.

The molecule OCS and its ions are known to be very stable, and even the lifetime of the triply charged cation OCS^{3+} had been shown by mass-spectrometry studies to be of the order of a few microseconds.[2] Very recently, Eland *et al.* have calculated the potential-energy surfaces of a large number of states of the latter species[3] confirming the observation of metastable OCS^{3+}. For the ground states of dicationic OCS^{2+} Ridard *et al.* have calculated in the 1980s a lifetime of 10^{160} s.[4] Thirty years later a large number of metastable states were theoretically predicted for OCS^{2+} by Brites *et al.*[5] This high stability of the molecule with respect to dissociation is due to several occupied non-bonding or anti-bonding valence orbitals, i.e., even the creation of two or three holes in the valence shell results in states with a bonding character.

Despite this high stability of the molecule that is responsible for the large number of metastable dicationic states, only very little is known from experiments about their potential-energy surfaces. This is due to the fact that rovibrational spectroscopy on OCS^{2+} is hard to perform due to the fact that only a low target density can be achieved in such experiments. As an alternative, OCS^{2+} dications can be studied by single photon double ionization.[6] The resulting spectra, however, are difficult to analyze since the transition probabilities depend strongly on bond distances, i.e., the Franck-Condon approximation is no more adequate. As a consequence, a simple analysis of vibrational profiles based on the Franck-Condon principle is hardly possible. This limitation in the data analysis can be overcome by using a sequential double ionization, where the first ionization process creates a core hole and the second one is the subsequent Auger decay. In this case, vibrationally resolved Auger-electron spectra provide detailed information on the potential-energy surfaces of the dicationic final states.[7–9] To our knowledge, the most complete theoretical study of bound vibrational states of Auger transitions of a polyatomic molecule has been made for the water molecule by Cesar *et al.*[10] This group of authors showed how multi-dimensional vibrations can be treated in a rigorous way, i.e., how a modification of the vibrational progressions, caused by a mixing of the various vibrational modes induced by the electronic transition, can be described by applying the so-called Dushinsky transformation.[11]

The Auger-electron spectrum (AES) of OCS subsequent to S $2p^{-1}$ photoionization had been studied before by Carroll *et al.*[12] More recently, Bolognesi *et al.*[13] reported a photoelectron-Auger-electron coincidence spectrum, while Kaneyasu *et al.*[14] presented the results of Auger-electron-ion coincidence measurements. These three publications, however, are limited by relatively moderate energy resolution

a)Present address: Institut für Physikalische und Theoretische Chemie, Universität Tübingen, Auf der Morgenstelle 18, D-72076 Tübingen, Germany.
b)Present address: Institut für Experimentalphysik, Universität Hamburg, Luruper Chaussee 149, D-22761 Hamburg, Germany.
c)Present address: Shanghai Advanced Research Institute, Chinese Academy of Sciences, Pudong, Shanghai 201210, China.

of the AES. Complementary calculations of the AES had been reported by Carroll *et al.*[12] and by Minelli *et al.*[15] On the other hand, several studies exist of resonant AES (Ref. 16–18) as well as of resonant X-ray fluorescence spectra of this molecule.[18–20] In this context, a core-excited state of the sulphur atom with an exceptionally long core-hole lifetime had been observed.[18,19]

In the present work, we present a high-resolution AES that exhibits vibrational structures for eight transitions. These fine structures are assigned to C−O or C−S stretching vibrational modes, and a Franck-Condon analysis allows to derive detailed information on the potential-energy surfaces. We also present new calculations for the AES that take spin-orbit and ligand-field splitting as well as the various orientations of the three S $2p^{-1}$ core-hole states into account. These theoretical spectra result in different intensity ratios for the Auger transitions and are therefore very helpful in the process of assigning the observed transitions. In this way, we obtained a clear picture of the potential-energy surfaces of the metastable dicationic final states of OCS, and we compared the results with recent theoretical predictions.[5] In addition, we performed a Franck-Condon analysis of the photoelectron spectrum (PES) and derived the geometry of the S $2p^{-1}$ core-hole state.

II. EXPERIMENTAL SETUP

The PES and AES of OCS were recorded at the gas-phase beamline I411 of the 1.5-GeV electron storage ring Max II in Lund, Sweden.[21] The measurements were performed with photon energies of 200, 220, and 240 eV. The PES were taken with a photon-energy resolution (full width at half maximum, FWHM) of $\simeq$15 meV using a 10-μm exit slit for the monochromator. The AES was recorded at a much lower photon-energy resolution (of $\simeq$0.6 eV) in order to increase the count rates, since the photon-energy resolution of the excitation process does not contribute to the total energy resolution of an AES. The experimental endstation at this beamline was equipped with a high-resolution Scienta SES-200 hemispherical electron analyzer that could be rotated in the plane perpendicular to the incoming beam. All spectra were collected at the magic angle of 54.7°, with the electrons entering the analyzer retarded to a pass energy of 10 eV, corresponding to a kinetic-energy resolution of $\simeq$20 meV. The PES was calibrated by assuming a value of 171.93(3) eV for the ionization energy of the S $2p_{1/2}$ level as published by Coville *et al.*,[22] while the AES was calibrated by using the value of 37.76(3) eV for the double-ionization energy of the $2^1\Pi$ dicationic state as reported by Eland.[6] This spectral feature could be related to lines in the present AES – independent of the assignment – by comparing the present experimental energy separation of the states assigned to *B* and $2^3\Pi$ as well as the splitting of the latter state by $\simeq$40 meV with the values for the states $2^1\Pi$ and $2^3\Pi$ reported by Eland.[6] In this way, the kinetic-energy scale could be calibrated with an accuracy of 60 meV. The OCS gas, with a purity of 97.5%, used in the present studies was purchased from Sigma-Aldrich Chemie GmbH; its purity was checked by PES recorded in the valence region in order to detect possible impurities, such as water.

III. DATA ANALYSIS AND THEORETICAL PROCEDURE

OCS is a linear triatomic molecule with three different vibrational modes. In the present study, it turned out that only the C−O stretching vibrational mode v_1 and the C−S stretching vibrational mode v_3 contribute to the PES as well as the AES. In the following, we label the vibrational substates with $v = (v_1 v_3)$. In addition, throughout this work, $v'' = (00)$ indicates the vibrational ground state of the electronic ground state, v' the vibrational levels of the S $2p^{-1}$ core-ionized states, and v the vibrational levels of the dicationic final states.

The data analysis procedure had already been described in a previous publication.[7] Here, we summarize only the major ideas and describe differences from the previous procedure. The AES and PES taken at the same photon energy were fitted simultaneously using the same set of parameters when applicable. This allowed us to describe both the PES and the AES with a relatively low number of free fit parameters, increasing the reliability of the fit results for the common parameters. Spin-orbit and molecular-field splittings were taken into account in the fit procedure, as well as post-collision interaction (PCI) and vibrational structures.

Since the energy splittings between the S $2p^{-1}_{3/2,1/2}$ and S $2p^{-1}_{3/2,3/2}$ intermediate states and those of the vibrational substates of the various S $2p^{-1}$ core-ionized states are of the same order of magnitude as the lifetime width Γ, the process cannot be described in a two-step model. Consequently, the excitation and de-excitation processes were described in a one-step model according to the Kramers-Heisenberg formula,[23] taking vibrational lifetime interferences into account.

The relative intensities of the transitions to the various vibrational sublevels are given by the Franck-Condon factors, i.e., the squares of the overlap integrals formed by the vibrational wave functions of the two electronic states involved in the transition. To calculate the overlap integrals, the potentials of the ground state, the intermediate S $2p^{-1}$ core-ionized state, and the various final states were assumed to be of the Morse type; possible differences in the potential-energy surfaces of the various spin-orbit and molecular-field components of the S $2p^{-1}$ core-ionized state were neglected. Apart from the energy zero point, a Morse potential is defined by the three parameters (i) vibrational energy $\hbar\omega$, (ii) anharmonicity $x\hbar\omega$, and (iii) equilibrium distance along the corresponding normal coordinate Q. Based on these three parameters for each Morse potential, the overlap integral of an electronic transition can be calculated, using an algorithm based on the work of Halmann and Laulicht[24] as well as Ory *et al.*[25] Values for the potential-energy surface of the ground state were taken from Ref. 26. The three parameters of the Morse potentials of the S $2p^{-1}$ intermediate and the various final states were varied in each iteration step during the fit analysis in order to improve the consistency with the experimental results. In the PES, only the C−O stretching vibrational mode can be observed, while some Auger transitions show also the C−S stretching vibrational mode requiring a two-dimensional Franck-Condon analysis. For Auger transitions with energies between 132 and 135 eV that exhibit both the C−S and the C−O stretching vibrational modes, the contributions from the C−S stretching vibrational mode turned out to be very small.

In these cases, vibrational substates with $v_3 = 1$ could only be observed, but no higher ones. Therefore, the Franck-Condon analysis of the C−S stretching vibrational mode could be simplified by appling the relation $\frac{I(v'=(00)\rightarrow v=(01))}{I(v'=(00)\rightarrow v=(00))} = \frac{(\Delta Q_3)^2\omega_3}{2\hbar}$.[27] Here, $\frac{I(v'=(00)\rightarrow v=(01))}{I(v'=(00)\rightarrow v=(00))}$ is the intensity ratio of Auger transition to vibrational levels with $v_3 = 1$ to those with $v_3 = 0$. ΔQ_3 is the change of the normal coordinate related to the C−S stretching vibrational mode and ω_3 stands for the vibrational frequency of the C−S stretching vibrational mode. The model underlying this description[27] is based on harmonic potentials with identical frequencies for the two electronic states involved and it neglects anharmonicities. However, in the present case of small $\frac{I(v'=(00)\rightarrow v=(01))}{I(v'=(00)\rightarrow v=(00))}$ ratios the loss of accuracy due to this approximation is marginal, while the required computer time for the fit analysis is substantially reduced.

In the present analysis, all calculations of the vibrational matrix elements were not performed in real space, but in the space of the normal coordinates, resulting in changes of the normal coordinates, ΔQ, upon electronic transitions. Polyatomic molecules possess more than one normal coordinate, and – in general – the definite normal coordinate Q^i cannot be associated with a single bond equilibrium distance R_e^j or a single bond equilibrium angle γ_e^k. In order to convert changes of the normal coordinates to changes of the distances R_e(C−O) and R_e(C−S), we calculated the **L**-matrix that describes the relation between R_e^j and Q_i by $R_e^j = \mathbf{L_{ji}} Q_i$. Using an algorithm described in Ref. 28 as well as force constants for the ground state as reported in Ref. 26, we obtained

$$\begin{pmatrix} \Delta R(\mathrm{C-O}) \\ \Delta R(\mathrm{C-S}) \end{pmatrix} = \begin{pmatrix} 0.378(4) & -0.04(3) \\ -0.25(2) & -0.23(2) \end{pmatrix} \times \begin{pmatrix} \Delta Q_1 \\ \Delta Q_3 \end{pmatrix}. \quad (1)$$

Here Q_1 and Q_3 describe the C−O and the C−S stretching vibrational modes, respectively. The **L** matrix is different for individual states, and we estimated the error bars using the **L** matrix for the ground state of OCS as well as for the three lowest states of OCS^{2+}, namely $\tilde{X}^3\Sigma^-$, $\tilde{a}^1\Delta$, and $\tilde{b}^1\Sigma^+$, as calculated by Hochlaf.[29] Taking the large error bars of the matrix elements into account, we present values not only for equilibrium distances in real space, but also for changes of the equilibrium distances in normal coordinates, ΔQ. These values are much more accurate and allow to repeat the conversion into real space using an improved **L** matrix, that could be obtained by more sophisticated calculations.

For both PES and AES, post-collision interaction (PCI) effects have to be taken into account. To achieve this, the lines in the PES as well as the direct terms in the Kramers-Heisenberg equation that describes the AES, can be approximated by a lineshape first given by Kuchiev and Sheinerman;[30] in the present work it is used in a simplified form given by Armen *et al.*[31] For the less important cross terms, we use the line shape given by the corresponding terms of the Kramers-Heisenberg equation by including an average energy shift to approximate the photoelectron relaxation. The lineshapes in the PES [AES] were convoluted with a Gaussian of ≃30 [40] meV full-width-half-maximum (FWHM), to account for experimental resolution.

The background in the AES consists of a parabolic line as well as a number of broad Gaussian lines that describe Auger transitions to states revealing no vibrational structure, i.e., states that are unstable with respect to dissociation. The widths of the Gaussian lines were treated as free parameters in the fit analysis. The obtained values are, however, much larger than the lifetime broadening of the narrow lines studied in the Franck-Condon analysis. Because of this, the broad Gaussian lines represent a smoothly varying background with negligible influence on the results of the Franck-Condon analysis. This negligible influence can be understood by the fact that the energy positions and intensities of the individual vibrational substates of a vibrational progression are strongly correlated, see Ref. 32. As a consequence, minor insufficiencies in the description of the background will not lead to different values of those fit parameters (within the present level of accuracy) that are relevant to the Franck-Condon analysis.

Auger transition rates of the S $2p^{-1}$ core-ionized OCS molecule were obtained with the so-called one-center approach.[33–36] To this end, the OCS molecule was calculated with C−O and C−S bond lengths of 1.124 and 1.581 Å, respectively, i.e., the values determined from the present PES, see below. To estimate the influence of the equilibrium distances on the theoretical results, we also performed calculations using parameter values at the limits of the error bars, see also below, and we found no significant changes of the energy positions and Auger intensities. The calculations were carried out with the cc-pVDZ basis set.[37] The occupied orbitals were determined at the Hartree-Fock level, and virtual valence orbitals were obtained with the improved-virtual-orbitals approach as described in Ref. 38. Auger transition rates were determined as in Ref. 36 using the Auger transition integrals of Chen *et al.*[39] and the known spin-orbit splitting parameters[18,40] of this molecule. The results for final states relevant to this work are collected in Table I, while the data for the complete set of the calculated final states is available in the supplementary material of this article.[41]

IV. S $2p^{-1}$ PES OF THE OCS MOLECULE

The configuration of the OCS molecule in the electronic ground state is

$$(1\sigma)^2(2\sigma)^2(3\sigma)^2(4\sigma)^2(5\sigma)^2(1\pi)^4,$$
$$(6\sigma)^2(7\sigma)^2(8\sigma)^2(2\pi)^4(9\sigma)^2(3\pi)^4,$$

where the first four orbitals represent the core electrons S $1s^2$, O $1s^2$, C $1s^2$, and S $2s^2$, respectively. The orbitals 5σ and 1π are the result of molecular-field splitting of the S $2p$ core level (in this description the spin-orbit splitting of the S $2p$ level is neglected). The remaining orbitals describe the valence shell of the molecule.

The PES as well as the AES (see below) of the OCS molecule were measured with photon energies of 200, 220, and 240 eV revealing no significant energy dependence. Furthermore, the fit results obtained for the three different excitation energies turned out to be rather similar. Therefore, the presented fit parameters are average values for the three

TABLE I. Results of the present calculations for selected dicationic states in OCS; for complete Table see supplementary material.[41] For each final state, the leading configuration and its contribution (in %) are listed, where the leading configuration is defined by the occupancy of the molecular orbitals relative to the ground-state configuration of neutral OCS. In addition, the energies E relative to the ground state $\tilde{X}^3\Sigma^-$ of dicationic OCS^{2+} as well as the Auger transition rates for the three different core-hole states are given. For better comparison with the figures and the other tables in this publication, the final states with Auger intensities significantly different from zero are labeled with the letters *a* to *o*.

		Configuration							Auger rates (10^{-6} a.u.)		
Dicationic state	Label	Changes					(%)	E (eV)	S $2p_{1/2}^{-1}$	S $2p_{3/2,1/2}^{-1}$	S $2p_{3/2,3/2}^{-1}$
$\tilde{X}^3\Sigma^-$	*a*				$3\pi^{-2}$		90.13%	0.000	267.21	204.06	471.27
$\tilde{a}^1\Delta$	*b*				$3\pi^{-2}$		87.75%	1.003	278.98	219.00	472.80
$\tilde{b}^1\Sigma^+$	*c*				$3\pi^{-2}$		84.44%	1.503	149.89	117.40	254.88
$1^1\Sigma^-$			$2\pi^{-1}$		$3\pi^{-1}$		84.99%	3.574	0.03	0.02	0.05
$1^3\Delta$			$2\pi^{-1}$		$3\pi^{-1}$		88.71%	3.862	0.18	0.13	0.31
$1^3\Sigma^+$			$2\pi^{-1}$		$3\pi^{-1}$		89.61%	3.976	0.10	0.08	0.16
$2^3\Sigma^-$	*d*		$2\pi^{-1}$		$3\pi^{-1}$		69.08%	4.546	40.85	31.20	72.05
$1^3\Pi$	*e*			$9\sigma^{-1}$	$3\pi^{-1}$		80.08%	5.169	270.88	268.04	280.02
$2^1\Delta$	*f*		$2\pi^{-1}$		$3\pi^{-1}$		68.45%	5.573	65.40	51.23	111.20
$1^1\Pi$	*g*			$9\sigma^{-1}$	$3\pi^{-1}$		49.41%	6.096	88.42	86.42	94.90
$2^1\Sigma^+$	*h*		$2\pi^{-1}$		$3\pi^{-1}$		68.65%	6.256	39.40	30.98	66.60
$2^3\Pi$	*i*	$8\sigma^{-1}$			$3\pi^{-1}$		76.10%	6.672	79.22	72.48	101.02
$2^1\Pi$	*j*	$8\sigma^{-1}$			$3\pi^{-1}$		38.91%	7.410	93.78	85.76	119.76
$^1\Sigma^-$					$3\pi^{-3}$	$4\pi^1$	61.38%	8.255	0.01	0.00	0.01
$^3\Delta$					$3\pi^{-3}$	$4\pi^1$	57.30%	8.256	0.03	0.01	0.04
$^3\Sigma^+$					$3\pi^{-3}$	$4\pi^1$	60.91%	8.386	0.00	0.00	0.00
$^3\Sigma^-$			$2\pi^{-1}$		$3\pi^{-2}$	$4\pi^1$	93.24%	8.527	0.32	0.25	0.57
$^3\Delta$			$2\pi^{-1}$		$3\pi^{-2}$	$4\pi^1$	92.15%	8.798	0.00	0.00	0.00
$^3\Pi$	*k*		$2\pi^{-1}$	$9\sigma^{-1}$			74.15%	9.387	37.52	34.84	46.14
$^3\Sigma^+$			$2\pi^{-1}$		$3\pi^{-2}$	$4\pi^1$	96.52%	9.394	0.00	0.00	0.00
$^3\Sigma^+$			$2\pi^{-1}$		$3\pi^{-2}$	$4\pi^1$	93.48%	9.809	0.00	0.00	0.00
$^3\Delta$			$2\pi^{-1}$		$3\pi^{-2}$	$4\pi^1$	96.01%	9.970	0.00	0.00	0.00
$^3\Gamma$			$2\pi^{-1}$		$3\pi^{-2}$	$4\pi^1$	97.71%	9.985	0.00	0.00	0.00
$^1\Delta$			$2\pi^{-1}$		$3\pi^{-2}$	$4\pi^1$	94.39%	9.990	0.59	0.46	1.00
$^3\Sigma^-$			$2\pi^{-2}$				60.76%	10.069	0.40	0.31	0.71
$^1\Sigma^+$			$2\pi^{-1}$		$3\pi^{-2}$	$4\pi^1$	95.07%	10.409	0.43	0.37	0.65
$^1\Pi$	*l*		$2\pi^{-1}$	$9\sigma^{-1}$			55.90%	10.424	95.00	87.60	118.92
$^1\Sigma^+$	*m*	$8\sigma^{-1}$		$9\sigma^{-1}$			51.99%	11.014	16.22	20.79	1.44
$^3\Pi$	*n*		$2\pi^{-1}$	$9\sigma^{-1}$	$3\pi^{-1}$	$4\pi^1$	57.80%	14.352	13.06	11.02	19.72
$^1\Sigma^+$	*o*			$9\sigma^{-2}$			54.38%	15.164	143.90	177.67	34.83

photon energies. The quoted error bars are based on the scattering of the values obtained for the different photon energies, but not on the statistical error bars resulting from the fit procedure; these latter values are unphysically small, since they are not taking into account small insufficiencies of the fit model, like, e.g., the fact that vibrational modes that are not clearly observed have been omitted (see, e.g., the C−S stretching vibrational mode in the PES).

The PES of the OCS molecule at the S $2p$ ionization threshold obtained with 200-eV photons is shown in Fig. 1. Due to spin-orbit interaction and molecular-field splitting, the three well-known core-hole states S $2p_{1/2}^{-1}$, S $2p_{3/2,1/2}^{-1}$, and S $2p_{3/2,3/2}^{-1}$ are observed. In the first fit approach, we assumed different potential-energy surfaces for these three states. However, we found no significant differences in the fit parameters, and therefore we used identical potential-energy surfaces for all three states in our analysis reducing the CPU-time considerably. The high quality of the fit shown in Fig. 1 demonstrates that one vibrational progression for each core-hole state is sufficient to describe the spectrum well.

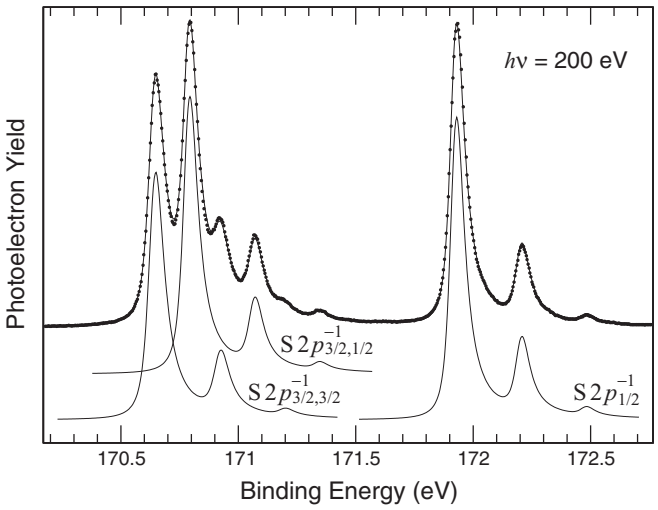

FIG. 1. S $2p^{-1}$ PES of OCS recorded at a photon energy of 200 eV. The solid line through the data points represents the fit result, while the three subspectra represent the vibrational progressions of the three different core-hole states due to spin-orbit and molecular-field interaction.

A comparison with the well-known vibrational energies of the ground state of OCS (Ref. 26) shows that the vibrational progressions in the PES correspond to the C−O stretching mode. We, therefore, used in the fit analysis the following Morse parameters of the ground state: vibrational energy $\hbar\omega_1''$ = 257.13 meV and anharmonicity $x\hbar\omega_1''$ = 1.4321 meV.[26] In this way, the fit resulted in a vibrational energy of $\hbar\omega_1'$ = 280.8(4) meV and an anharmonicity of $x\hbar\omega_1'$ = 1.3(1) meV for the S $2p^{-1}$ core-ionized state. The result for $\hbar\omega_1'$ is in reasonable agreement with the value of $\hbar\omega_1'$ = 290.39 meV calculated by Siggel *et al.*[42] In addition, we obtained a splitting of 278.2(5) meV between the first two vibrational sublevels of the S $2p^{-1}$ states, a value that agrees well with the previous experimental result of 279 meV by Kukk *et al.*[43]

For the three core-hole states S $2p_{1/2}^{-1}$, S $2p_{3/2,1/2}^{-1}$, and S $2p_{3/2,3/2}^{-1}$ lifetime widths of 61(2), 64(2), and 68(2) meV, respectively, were derived. The slight differences can be qualitatively understood by the well-known dependence of the Auger rate and hence the lifetime broadening on the orientation of the core hole.[36,44,45]

The S $2p_{3/2,3/2}^{-1}$ core hole is π-oriented ($2p\pi^{-1}$),[46] i.e., it can be described by a hole in the 1π orbital. In contrast, the S $2p_{1/2}^{-1}$ core hole has 57% π- and 43% σ-contribution, while the S $2p_{3/2,1/2}^{-1}$ core hole has 43% π- and 57% σ-character ($2p\sigma^{-1}$, i.e., a hole in the 5σ orbital).[46] Assuming a higher Auger rate for a $2p\pi^{-1}$ core hole as compared to a $2p\sigma^{-1}$ core hole and considering the similar orientations of the S $2p_{1/2}^{-1}$ and S $2p_{3/2,1/2}^{-1}$ core holes (both are roughly 50% $2p\sigma^{-1}$ and 50% $2p\pi^{-1}$), we can understand qualitatively that their lifetime broadenings are rather similar, while the lifetime broadening of the S $2p_{3/2,3/2}^{-1}$ core hole (100% $2p\pi^{-1}$) is larger. The present calculations result in a lifetime widths of 77 meV for the S $2p\pi^{-1}$ core hole and of 34 meV for the S $2p\sigma^{-1}$ core hole, resulting in lifetime widths of 59 meV, 52 meV, and 77 meV for the S $2p_{1/2}^{-1}$, S $2p_{3/2,1/2}^{-1}$, and S $2p_{3/2,3/2}^{-1}$ core-hole states, respectively. The calculated differences are clearly too large, but they correctly predict the similarities of the broadenings of the core holes S $2p_{3/2,1/2}^{-1}$ and S $2p_{1/2}^{-1}$, while that of the S $2p_{3/2,3/2}^{-1}$ core hole is larger, in qualitative agreement with observation. On the other hand, we can derive from the known core-hole orientations and the measured lifetime widths of the spin-orbit and ligand-field-split core-hole states lifetime broadenings of 68(2) meV for the $2p\pi^{-1}$ and of 58(4) meV for the $2p\sigma^{-1}$ core-hole state, respectively. These values for the lifetime broadening show that the present theoretical total $2p\sigma^{-1}$ Auger rate is considerably underestimated in comparison with the total $2p\pi^{-1}$ Auger rate. An analogous conclusion can be drawn from the branching ratios of the Auger transitions from different core holes to a given final state, see below.

The fit analysis of the present data resulted in a splitting of 1.1367(5) [1.2828(3)] eV between the S $2p_{1/2}^{-1}$ and the S $2p_{3/2,1/2}^{-1}$ [S $2p_{3/2,3/2}^{-1}$] core holes, in good agreement with previous experimental values of 1.1395(5) [1.2845(5)] eV as reported by Kukk *et al.*[43] The relative intensities of the core-hole states S $2p_{1/2}^{-1}$, S $2p_{3/2,1/2}^{-1}$, and S $2p_{3/2,3/2}^{-1}$ resulted in 0.33(1), 0.33(1), and 0.34(1), respectively, revealing no dependence on photon energy.

Furthermore, the fit of the PES allowed us to derive changes of the normal coordinate, ΔQ_1, associated with an excitation of the C−O stretching mode. By applying the **L** matrix given in Eq. (1), we obtained the following changes of the internal coordinates: ΔR_e(C−O) = −0.0330(8) Å and ΔR_e(C−S) = 0.021(2) Å. These values agree quite well with the results given by Kosugi and Ishida:[46] ΔR_e(C−O) = −0.041 Å and ΔR_e(C−S) = 0.042 to 0.049 Å; the different values for ΔR_e(C−S) are caused by the different core-hole states. The results demonstrate that S $2p^{-1}$ ionization causes a decrease in the C−O bond distance, while the C−S bond distance increases. The absolute numbers as well as the different C−S equilibrium distances for the various core-hole states could, however, not be reproduced in the present fit analysis.

Possible differences in the C−S distances can be associated with very weak and therefore unobserved excitations of the C−S stretching vibrational mode. From the data analysis, we can give an upper limit of 0.01 for the $\frac{I(v'=(00)\rightarrow v=(01))}{I(v'=(00)\rightarrow v=(00))}$ intensity ratio. This results in an upper limit of 0.007 Å for possible corrections of both the C−S and the C−O bond distances. Since possible excitations of the C−S stretching vibrational mode can be different for the various core-hole states, the presented upper limit of such contributions does not exclude differences up to 0.007 Å for the equilibrium distances of the various core-hole states as predicted by Kosugi and Ishida.[46] By using ground-state equilibrium distances of R_e(C−O) = 1.157 Å and R_e(C−S) = 1.560 Å,[26] we obtain R_e(C−O) = 1.124(8) Å and R_e(C−S) = 1.581(9) Å for all core-ionized states. These values were used for the present calculations of the Auger spectra, as described above.

V. S $2p^{-1}$ NORMAL AUGER-ELECTRON SPECTRUM OF THE OCS MOLECULE

The upper part of Fig. 2 presents the S $2p^{-1}$ normal AES of OCS in the kinetic-energy region from 125 to 143 eV, i.e., the region where a previous publication[12] had reported medium-resolution spectra with structures of a total width of ≃1 eV. The theoretical results of the present work are displayed in the lower part of the figure; here, the accuracy of the relative theoretical energy positions is estimated to be of the order of 1 eV. Note that the theoretical spectrum is obtained by convoluting all transition rates with a Gaussian of the same width, while the experimental line shapes are different for the individual transitions. Consequently, the peak heights cannot be compared directly. However, the calculated transition rates turned out to be particularly helpful in assigning final states with peculiar branching ratios in the AES, see below.

Contrary to previous studies by Carroll *et al.*,[12] we resolved a number of narrow lines with a total width of ≃65 meV in the energy region from 128 to 135 eV. According to spacings of ≃250 meV, some of these lines (e.g., in the energy region from 129 to 132 eV) are assigned to the C−O stretching-vibrational mode of different Auger transitions. In addition, we observe splittings of ≃70 meV in the energy region from 138 to 141 eV as well as of ≃100 meV in the region from 132 to 135 eV (not visible in Fig. 2, see below); we assign them to an excitation of the C−S

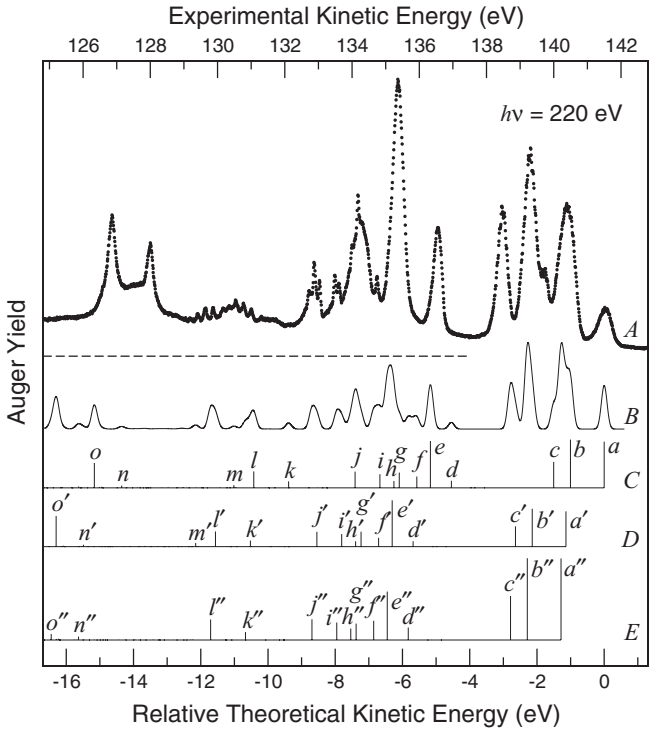

FIG. 2. Normal AES of the OCS molecule subsequent to S $2p^{-1}$ photoionization with 220-eV photons recorded in the kinetic-energy region from 125 to 143 eV (upper spectrum *A*, upper energy scale). The baseline of spectrum *A* is indicated by the dashed horizontal line. Spectrum B (lower energy scale, with kinetic energies relative to the S $2p_{1/2}^{-1} \rightarrow \tilde{X}^3\Sigma^-$ transition) represents the theoretical AES. The bar diagrams *C*–*E* represent the calculated partial AES originating from S $2p_{1/2}^{-1}$, S $2p_{3/2,1/2}^{-1}$, and S $2p_{3/2,3/2}^{-1}$ core holes, respectively. For a comparison with Table I and Table IV, Auger transitions to the same final state are marked with the same letter. In this context, transitions marked by prime and double prime refer to S $2p_{3/2,1/2}^{-1}$ and S $2p_{3/2,3/2}^{-1}$ core holes, while letters without further marking refer to a S $2p_{1/2}^{-1}$ core hole. Only intensities $\geq 10 \times 10^{-6}$ a.u. are marked by letters.

stretching-vibrational mode. In total, we observed eight Auger transitions with a vibrational progression, i.e., to metastable dicationic final states. The information about their potential-energy surfaces derived from the data analysis is summarized in Tables II and III.

To perform a Franck-Condon fit analysis of the vibrational progressions, this spectrum was divided into three regions that were treated separately. The first region from 138 to 142 eV consists of three final states of the $3\pi^{-2}$ configuration. The second region from 131.5 to 137.5 eV contains Auger transitions with vibrational progressions to four metastable final states, which are mainly assigned to the configurations $2\pi^{-1}3\pi^{-1}$, $9\sigma^{-1}3\pi^{-1}$, and $8\sigma^{-1}3\pi^{-1}$. The third region from 128.5 to 132 eV exhibits Auger transitions to the metastable final state $8\sigma^{-1}9\sigma^{-1}(^1\Sigma^+)$, on top of a rather intense smooth background. In the following, we shall discuss the three regions separately.

A. S $2p^{-1} \rightarrow 3\pi^{-2}$ Auger transitions

Figure 3 shows the spectrum of Auger transitions to the states $\tilde{X}^3\Sigma^-$, $\tilde{a}^1\Delta$, and $\tilde{b}^1\Sigma^+$ that belong all to the configuration $3\pi^{-2}$. This energy region is dominated by vibrational splittings of $\simeq$65 meV that can be assigned to excitations of the C−S stretching vibrational mode. This mode is clearly visible for transitions to the final states $\tilde{a}^1\Delta$ and $\tilde{b}^1\Sigma^+$, but it is much less pronounced for transitions to the final state $\tilde{X}^3\Sigma^-$. In the latter case, we observed only some weak structures with a splitting of 65(5) meV on top of the S $2p_{3/2}^{-1} \rightarrow \tilde{X}^3\Sigma^-$ transition at $\simeq$ 141.5 eV, see inset. These weak vibrational structures indicate that the $\tilde{X}^3\Sigma^-$ state is stable with respect to dissociation, in full agreement with the potential-energy surfaces presented in Ref. 5 and the experimental observation of OCS^{2+} in coincidence with the S $2p^{-1} \rightarrow \tilde{X}^3\Sigma^-$ Auger transitions.[14]

TABLE II. Equilibrium distances, $R_{e,\,exp}$, of the observed states derived from our fit analysis. For comparison, the values for the ground state, taken from Ref. 26, are included. The changes in the normal coordinates relative to those of the ground state, ΔQ, are also listed for future conversions into real space using improved **L** matrices. The calculated equilibrium distances, $R_{e,\,th}$, taken from Ref. 5 are also given. For an assignment of the states *A* and *B*, see text.

	$R_{e,\,exp}$ (Å)		$R_{e,\,th}$ (Å)		ΔQ (Å · u$^{1/2}$)	
State	C−O	C−S	C−O	C−S	C−O	C−S
Ground	1.157[a]	1.560[a]				
S $2p^{-1}$	1.124(8)	1.581(9)			− 0.087(1)	0
$\tilde{a}^1\Delta$	1.18(3)	1.74(2)	1.12	1.75	− 0.027(4)	− 0.758(5)
$\tilde{b}^1\Sigma^+$	1.17(2)	1.69(2)	1.13	1.71	− 0.037(4)	− 0.508(2)
$2^1\Delta$	1.15(4)	1.57(3)	1.24[b]	1.75[b]	− 0.03(8)	0
$2^3\Pi$	1.158(12)	1.583(11)	1.16[b]	...[b,c]	− 0.008(5)	− 0.090(5)
$2^1\Pi$			1.22[b]	1.58[b]		
B	1.155(14)	1.603(13)			− 0.023(5)	− 0.159(6)
$2^1\Sigma^+$			1.24[b]	1.70[b]		
A	1.126(12)	1.581(11)			− 0.08(1)	0
$^1\Sigma^+$	1.195(8)	1.535(9)			0.100(1)	0

[a]Values fixed in the fit analysis.
[b]Estimated from the potential-energy surfaces given in Ref. 5.
[c]No potential minimum in the calculated curve.

TABLE III. Vibrational energies, $\hbar\omega_{exp}$, and anharmonicities, $x\hbar\omega_{exp}$, for the observed states derived from the fit analysis. For reasons of comparison values for the ground state taken from Ref. 26 as well as vibrational energies, $\hbar\omega_{theo}$, and anharmonicities $x\hbar\omega_{theo}$, derived from the calculations of Brites *et al.*,[5] are included. The anharmonicities of the C−O stretching vibrational mode of the states $\tilde{a}^1\Delta$ and $\tilde{b}^1\Sigma^+$ were fixed to values derived from Ref. 5. For the assignment of *A* and *B*, see text.

	$\hbar\omega_{exp}$ (meV)		$x\hbar\omega_{exp}$ (meV)		$\hbar\omega_{theo}$ (meV)		$x\hbar\omega_{theo}$ (meV)	
State	C−O	C−S	C−O	C−S	C−O	C−S	C−O	C−S
Ground	257.13[a]	107.77[a]	1.4321[a]	0.49597[a]				
S $2p^{-1}$	280.8(4)	1.3(1)						
$\tilde{X}^3\Sigma^-$		65(5)			284.1[b]	63.0[b]	3.4716[b]	0.09[b]
$\tilde{a}^1\Delta$	267.3[a,b]	70.0(4)	2.3559[a,b]	0.0	267.3[b]	67.9[b]	2.3559[b]	0.35[b]
$\tilde{b}^1\Sigma^+$	255.7[a,b]	73.0(9)	2.7278[a,b]	0.0	255.7[b]	72.9[b]	2.7278[b]	0.47[b]
$2^1\Delta$	266(20)		2[a,c]					
$2^3\Pi$	259(1)	100[a,c]	2[a,c]					
B	262(1)	93(3)	2[a,c]					
A	280(4)		2[a,c]					
$^1\Sigma^+$	238.0(5)		0.16(13)					

[a]Values fixed the fit analysis.
[b]Calculated from the energy positions reported in Ref. 5.
[c]Estimated value.

For the Auger transitions S $2p^{-1} \rightarrow \tilde{a}^1\Delta$ and S $2p^{-1} \rightarrow \tilde{b}^1\Sigma^+$, a two-dimensional Franck-Condon analysis was performed, which revealed the presence of the C−O stretching vibrational mode, see below. In contrast to this, we were not able to obtain a reasonable fit for the S $2p^{-1} \rightarrow \tilde{X}^3\Sigma^-$ transition from our Franck-Condon approach. Because of this, we described these Auger transitions with an empirical lineshape that was derived from the well-separated S $2p_{1/2}^{-1} \rightarrow \tilde{X}^3\Sigma^-$ transition and which is presented as a subspectrum in Fig. 3.

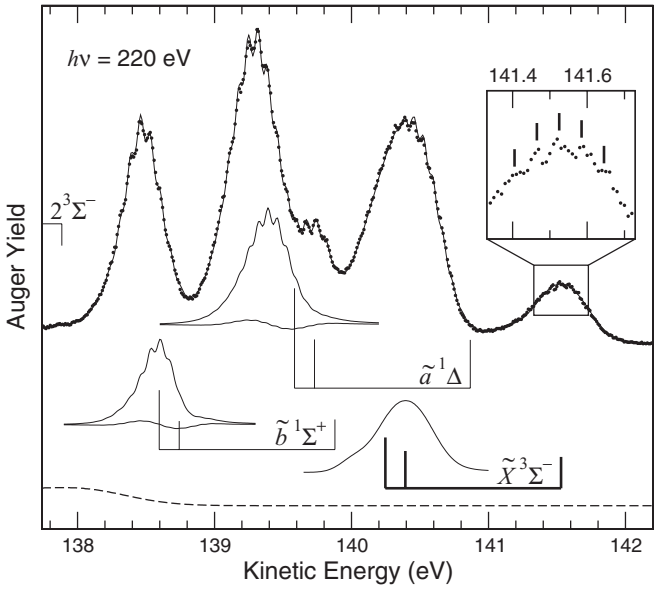

FIG. 3. Normal AES of the OCS molecule subsequent to S $2p^{-1}$ photoionization with 220-eV photons recorded in the kinetic-energy region from 137.75 to 142.2 eV. The solid line through the data points represents the fit result, while the dashed line represents the background. The energy positions of the $v' = (00) \rightarrow v = (00)$ transitions and the intensities of the spin-orbit and molecular-field split components of the transitions S $2p^{-1} \rightarrow \tilde{a}^1\Delta$ and S $2p^{-1} \rightarrow \tilde{b}^1\Sigma^+$ are marked by the thin vertical bars; the vibrational progression and vibrational lifetime interference contribution for the transition starting from the S $2p_{3/2,1/2}^{-1}$ core level are indicated by the upper and lower subspectra, respectively. The bold vertical-bar diagram indicates the intensities and the peak position of the transition S $2p^{-1} \rightarrow \tilde{X}^3\Sigma^-$; the corresponding subspectrum for the transitions starting from the S $2p_{3/2,1/2}^{-1}$ core hole represents the peak profile derived from our fit analysis. The inset displays the weak vibrational progressions of the S $2p^{-1} \rightarrow \tilde{X}^3\Sigma^-$ transition. The signal from the S $2p_{1/2}^{-1} \rightarrow 2^3\Sigma^-$ transition at ≃138 eV is contained in the dashed background.

The fact that the C−S stretching vibrational mode is only weakly pronounced in the S $2p^{-1} \rightarrow \tilde{X}^3\Sigma^-$ transition and that the Franck-Condon analysis failed in this case goes along with the observation of Brites *et al.*,[5] who reported that these vibrations were completely absent in their time-of-flight photoelectron-photoelectron coincidence (TOF-PEPECO) spectrum. For the S $2p^{-1} \rightarrow \tilde{a}^1\Delta$ transition, which could be described within the Franck-Condon approach in the present work, Brites *et al.* had observed a pronounced C−S stretching vibrational progression.[5] This comparison suggests that there is a link between the occurrence of a C−S stretching vibrational mode in the TOF-PEPECO spectra of Brites *et al.* and the possibility to describe the Auger transitions within a Franck-Condon approach.

Brites *et al.*[5] already excluded the possibilty that the C−S stretching vibrational mode could just be masked by a splitting of the $\tilde{X}^3\Sigma^-$ state into spin-orbit-split components $\tilde{X}^3\Sigma_0^-$ and $\tilde{X}^3\Sigma_1^-$, since they had calculated such a splitting to be of the order of 1 meV. This result is fully confirmed by the present calculations resulting in the same value. Brites *et al.* then suggested an indirect population of this final state by autoionization of excited OCS^{++}, possible under their experimental conditions, could mask the vibrational progression of the C−S mode. In the present experimental approach, however, such processes can be excluded. Therefore, we assume that the transitions to the $\tilde{X}^3\Sigma^-$ state exhibit a complicated and unresolved vibrational structure with contributions of the bending vibrational mode that might be caused by Fano resonances. However, more detailed calculations of the vibrational structures of transitions to the $\tilde{X}^3\Sigma^-$ state are necessary to clarify this question.

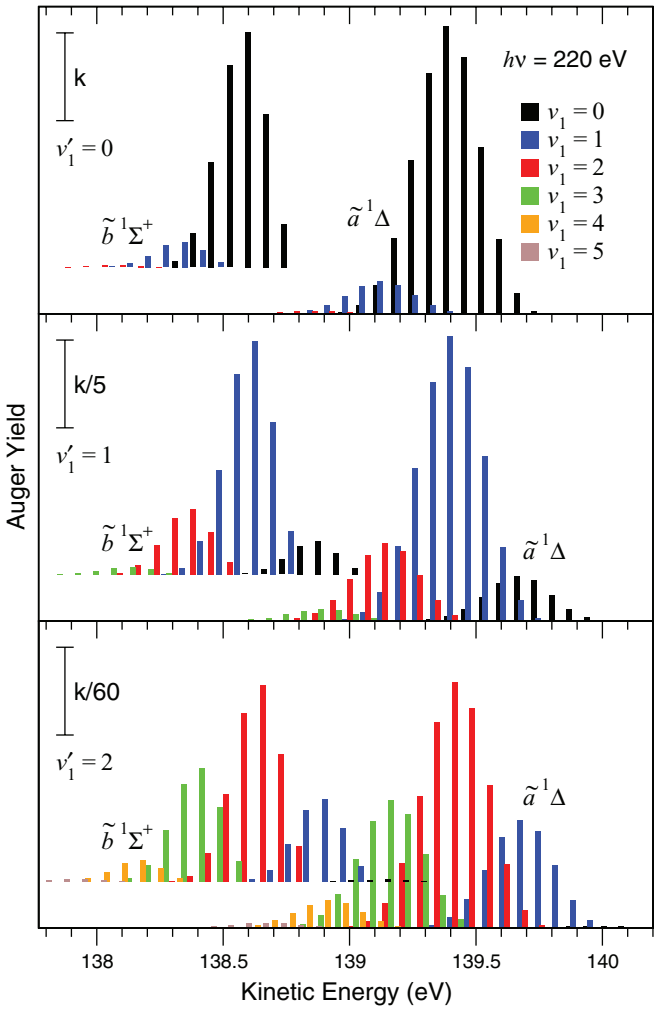

FIG. 4. Detailed vibrational structures of the S $2p_{1/2}^{-1} \rightarrow \tilde{a}^1\Delta$ and S $2p_{1/2}^{-1} \rightarrow \tilde{b}^1\Sigma^+$ Auger transitions as obtained from the fit analysis. The different frames distinguish the vibrational levels v_1' in the S $2p_{1/2}^{-1}$ core-hole state and the different colors describe the vibrational levels v_1 in the dicationic final state. The vertical bars of a certain color give for the two Auger transitions the vibrational progressions of the C−S stretching vibrational mode v_3 that belongs to fixed values of v_1' and v_1. The vibrational lifetime-interference contributions are not included in the progressions. The intensity ratios for the frames with $v_1' = 0$, 1, and 2, respectively, are 60 : 12 : 1.

The results of the two-dimensional Franck-Condon analysis of the S $2p^{-1} \rightarrow \tilde{a}^1\Delta$ and S $2p^{-1} \rightarrow \tilde{b}^1\Sigma^+$ transitions are shown in the subspectrum of Fig. 3. The $v' = (00) \rightarrow v = (00)$ transitions indicated by the thin vertical-bar diagrams are very weak and obviously not unambiguous, see also Fig. 4. To check the indicated energy positions, we shifted them by one quantum of the C−S stretching vibrational mode to lower and higher kinetic energies and repeated the fit analysis. However, all these fits resulted in considerably worse descriptions of the spectral features. The S $2p_{3/2}^{-1} \rightarrow \tilde{b}^1\Sigma^+$ transitions overlap partially with a structure in the background described by the dashed line in Fig. 3. The latter structure is assigned to the S $2p_{1/2}^{-1} \rightarrow 2^3\Sigma^-$ transition, see below.

Since the C−S stretching mode is not observed in the PES, we cannot determine the potential-energy surfaces along this coordinate. However, we can conclude that the changes are very small, see above, so that we can estimate the potential-energy surface of the S $2p^{-1}$ core-hole state along this coordinate by using the ground state values for the C−S stretching mode with a vibrational energy of $\hbar\omega_3'' = 107.77$ meV and an anharmonicity of $x\hbar\omega_3'' = 0.49597$ meV.[26]

The fit results are summarized in Tables II, III, and V, where the values for the equilibrium distances R_e(C−O) and R_e(C−S) as well as for the vibrational energies of the C−S stretching vibrational mode, $\hbar\omega_3$, agree quite well for both final states with those calculated by Brites *et al.*[5] The fit results for the anharmonicities of the C−S stretching vibrational mode, $x\hbar\omega_3$, are of the order of some 10^{-2} meV, i.e., much smaller than those predicted theoretically. We are not considering this as a contradiction, since in the present Franck-Condon analysis the anharmonicities could not be determined from measured energy positions of the vibrational substates, but only from intensity distributions. In fact the intensity distribution is substantially influenced by anharmonicity. In contrast to this, the effects of anharmonicity on the energy positions of the vibrational substates are way too small to be observed due to the large linewidths in core-level spectroscopy. The observed intensities – and hence also the fitted anharmonicites – can, however, be influenced by effects beyond the present approach, which simplifies the full three-dimensional potential-energy surfaces to two decoupled Morse potentials.

Fits using the vibrational energy of the C−O modes as a free parameter resulted for the two final states $\tilde{a}^1\Delta$ and $\tilde{b}^1\Sigma^+$ in $\hbar\omega_1 \simeq 240$ meV, which is 15–25 meV smaller than the values calculated by Brites *et al.*[5] Since these authors predicted the vibrational energies of the C−S stretching vibrational mode very well, see above, and since the excitations of the C−O vibrational mode are not directly observed in the present spectrum, we fixed in our fit analysis the vibrational energies and anharmonicities to the values derived from the energy positions given by Brites *et al.*, obtaining in this way a good description of the spectrum. In summary, the experimental findings are in good agreement with the potential-energy surfaces presented in Ref. 5.

The full complexity of the S $2p^{-1} \rightarrow \tilde{a}^1\Delta$ and the S $2p^{-1} \rightarrow \tilde{b}^1\Sigma^+$ Auger transitions, including the excitation of the C−O and C−S stretching modes, is displayed in Fig. 4. The figure shows that the vibrational progressions visible in Fig. 3 is mainly due to the $v' = (00) \rightarrow v = (0v_3)$ transitions. This is due to the fact that (i) the $v'' = (00) \rightarrow v' = (00)$ transition in the PES is the most intense one and (ii) the population of the higher vibrational substates $v' = (v_1'0)$ in the PES is distributed in the Auger decay to final states $v = (v_1v_3)$ with $v_1' \neq v_1$. In particular, we see for the S $2p_{1/2}^{-1} \rightarrow \tilde{a}^1\Delta$ Auger transitions, starting from $v' = (20)$, strong transitions to the vibrational levels $v = (1v_3)$, $(2v_3)$, and $(3v_3)$.

B. S $2p^{-1}$ Auger transitions to the configurations $2\pi^{-1}3\pi^{-1}$, $9\sigma^{-1}3\pi^{-1}$, and $8\sigma^{-1}3\pi^{-1}$

Figure 5 shows the AES in the kinetic-energy region from 131.4 to 137.5 eV, which consists of nine spin-orbit and ligand-field split transitions. Five of the transitions result

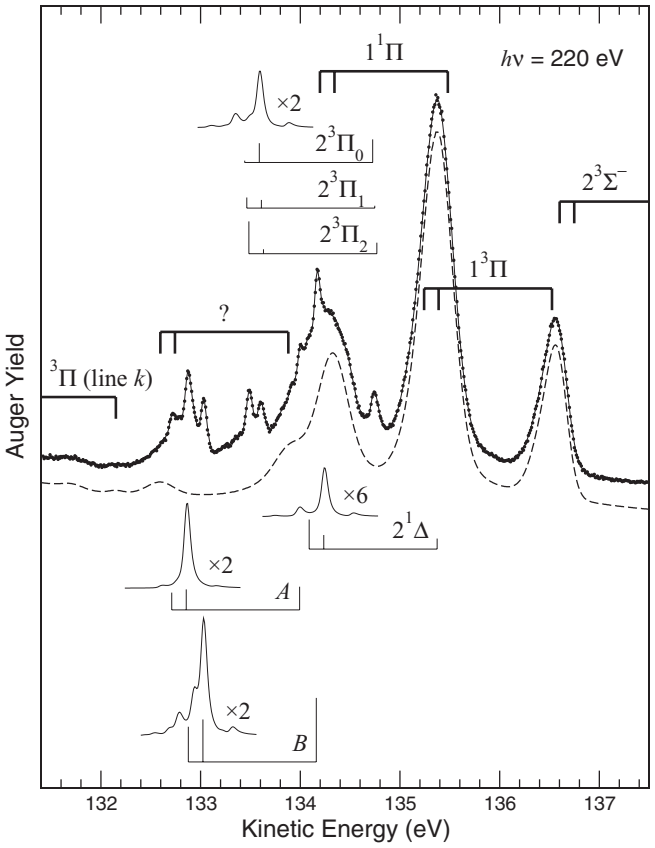

FIG. 5. Normal AES of the OCS molecule subsequent to S $2p^{-1}$ photoionization with 220-eV photons recorded in the kinetic-energy region from 131.4 to 137.5 eV. The dashed subspectrum indicates the contributions of Auger transitions to dissociative final states forming the background of the fit analysis and the bold bar diagrams indicate their approximate energy positions. For the metastable final states $2^1\Delta$, $2^3\Pi_{2,1,0}$, B, and A the energy positions of the $v' = (00) \rightarrow v = (00)$ transitions as well as the intensities of the Auger transitions starting at the various core-hole states are indicated by the thin vertical-bar diagrams. The subspectra display the vibrational progressions of the corresponding Auger transitions starting from the S $2p_{3/2,\,1/2}$ sublevel. For details concerning the assignment of A and B, see text.

in a dissociation of the molecule, see bold bar diagrams and dashed subspectrum. The remaining four transitions result in a metastable dicationic final state; they are indicated by the thin bar diagrams and by the solid subspectra. In the following, we shall first discuss the assignment of the transitions and subsequently the obtained fit results.

1. Assignment of transitions

To assign the observed Auger transitions, the present theoretical results for the energy region from 132.5 to 137.5 eV as well as those from literature[5,15] are summarized in Table IV. In this energy region the agreement between experiment and theory is, however, not sufficient for an unequivocal assignment. This holds in particular for the energy region from 132.5 to 134.2 eV, where not even tentative assignments can be presented. The most striking difference between experiment and theory in the energy region from 132.5 to 137.5 eV is the fact that Auger transitions to eight final states ($2^3\Sigma^-$, $1^3\Pi$, $1^1\Pi$, $2^1\Delta$, $2^3\Pi$, A, B, and ?) are observed experimentally, while the present calculations as well as the results of Minelli *et al.*[15] predict only seven Auger-transition rates significantly different from zero, namely those for transitions to the final states $2\pi^{-1}3\pi^{-1}$ ($2^3\Sigma^-$, $2^1\Delta$, and $2^1\Sigma^+$), $9\sigma^{-1}3\pi^{-1}$ ($1^3\Pi$ and $1^1\Pi$), and $8\sigma^{-1}3\pi^{-1}$ ($2^3\Pi$ and $2^1\Pi$). These seven transitions are marked by the letters d to j in Fig. 2 as well as in Tables I and IV. The present sequence of states with decreasing kinetic energy (increasing E in Table IV) from $2^3\Sigma^-$, $1^3\Pi$, $2^1\Delta$, $1^1\Pi$, $2^1\Sigma^+$, $2^3\Pi$, to $2^1\Pi$ is in full agreement with the results of Brites *et al.*[5] In the sequence of Minelli *et al.*, however, the order of the two states $2^3\Pi$ and $2^1\Sigma^+$ is exchanged.[15] The obvious contradiction between eight experimentally observed spin-orbit-split and ligand-field split Auger transitions and the seven theoretically predicted Auger transitions requires an assignment beyond the above listed sequence of transitions, see below.

In a first step, we identified the S $2p_{3/2}^{-1}$ components of the Auger transitions by employing the experimental S $2p_{3/2}^{-1}$ AES obtained from the photoelectron-Auger-electron coincidence work of Bolognesi *et al.*;[13] their spectrum displays four sharp peaks in the energy region from 131.5 to 137.5 eV. According to their fit analysis, these peaks are split by 5.11 eV, 6.03 eV, 6.72 eV, and 7.28 eV from the S $2p_{3/2}^{-1} \rightarrow \tilde{X}^3\Sigma^-$ transition, which – in the present energy scale – corresponds to 135.22 eV, 134.30 eV, 133.61 eV, and 133.05 eV, respectively.

The two peaks at 135.22 eV and 134.30 eV are in the energy region, where the present high-resolution spectrum is dominated by broad peaks due to dissociation. The energy positions of the two peaks reported by Bolognesi *et al.* as well as the resulting energy positions of the S $2p_{1/2}^{-1}$ Auger

TABLE IV. Comparison of the present theoretical results for the kinetic-energy region from 132.4 to 137.5 eV with the results of Minelli *et al.*[15] and Brites *et al.*[5] The energies, E, are given relative to the ground state $\tilde{X}^3\Sigma^-$ of OCS^{2+}; the total S $2p^{-1}$ Auger intensities, I_{norm}, are normalized to the S $2p^{-1} \rightarrow 1^3\Pi$ Auger transition.

		Present results		Ref. 15		Ref. 5
State	Label	E (eV)	I_{norm}	E (eV)	I_{norm}	E (eV)
$2^3\Sigma^-$	d	4.55	0.18	4.71	0.22	4.59
$1^3\Pi$	e	5.17	1.00	4.85	1.00	4.88
$2^1\Delta$	f	5.57	0.28	5.70	0.33	5.59
$1^1\Pi$	g	6.10	0.33	5.93	0.42	5.93
$2^1\Sigma^+$	h	6.26	0.17	6.46	0.25	6.36
$2^3\Pi$	i	6.67	0.31	6.45	0.30	6.64
$2^1\Pi$	j	7.41	0.37	7.28	0.45	7.30

transitions are indicated in Fig. 5 by the bold vertical-bar diagrams (labeled $1^3\Pi$ and $1^1\Pi$).

The peak at 135.22 eV had been assigned by Bolognesi *et al.* to S $2p_{3/2}^{-1} \rightarrow 1^3\Pi$ due to its high intensity in agreement with the calculations of Minelli *et al.*;[15] this assignment is also fully in line with the present theoretical results and shows that this transition forms the low-kinetic-energy part of the peak at 135.4 eV in the present spectrum, see Fig. 5.

According to the calculations presented in Table IV, the S $2p_{3/2}^{-1} \rightarrow 2^3\Sigma^-$ transition should be at kinetic energies that are 0.15–0.6 eV higher than those of the S $2p_{3/2}^{-1} \rightarrow 1^3\Pi$ transition, and it should be intense enough to be visible in the spectrum. Unfortunately, the S $2p_{3/2}^{-1}$ AES from Bolognesi *et al.*[13] is too noisy in the respective energy region to allow an identification of this transition. In the present spectrum, we also do not find any structure that can be assigned clearly to the S $2p_{3/2}^{-1} \rightarrow 2^3\Sigma^-$ transition. Assuming that the calculated intensities for this transition are in the right order of magnitude, we have to conclude that the S $2p_{3/2}^{-1} \rightarrow 2^3\Sigma^-$ transition overlaps almost perfectly either with the S $2p_{1/2}^{-1} \rightarrow 1^1\Pi$ transition or the S $2p_{1/2}^{-1} \rightarrow 1^3\Pi$ transition. From these two possible explanations we prefer an overlap with the S $2p_{1/2}^{-1} \rightarrow 1^3\Pi$ transition at 136.5 eV, since such an assignment would also explain the broad peak in the background of Fig. 3. This assignment would result in a splitting of 1.3 eV between the states $1^3\Pi$ and $2^3\Sigma^-$, which is by 0.7–1.1 eV larger than the theoretical splittings summarized in Table IV; we consider these numbers as an estimate for the accuracy of the theoretical relative energy values presented in Table IV.

The peak at 134.30 eV shows three S $2p_{3/2}^{-1}$ Auger transitions in the high-resolution AES presented in Fig. 5, namely a broad and intense peak that overlaps on its low-energy tail with two ligand-field split weak and narrow peaks. In addition, a strong and narrow peak is observed in the present spectrum at 134.16 eV, originating from the S $2p_{1/2}^{-1} \rightarrow B$ transition, see below. In the discussed energy region, all calculations predict the S $2p_{3/2}^{-1}$ Auger transitions to the final states $2^1\Delta$ and $1^1\Pi$, with the $2^1\Delta$ Auger transitions having slightly lower intensities and slightly higher kinetic energies, see Table IV. The experimental intensity ratio for these two states is obviously not reproduced by the calculations, i.e., the theoretical results might not be highly reliable for these states, see below. Based on the calculated potential-energy surfaces of Brites *et al.*,[5] we expect that the $2^1\Delta$ final state is metastable, while the $1^1\Pi$ final state is dissociative. As a consequence, we suggest that the broad peaks at higher kinetic energies are due to S $2p_{3/2}^{-1} \rightarrow 1^1\Pi$ Auger transitions, while the narrow peaks are due to S $2p_{3/2}^{-1} \rightarrow 2^1\Delta$ Auger transitions. We shall show further below that the potential-energy surfaces calculated for this energy region by Brites *et al.*[5] are not very accurate, see in particular the state $2^3\Pi$. All these deviations from experiment can readily be explained by avoided level crossings that have not been taken into account with sufficient accuracy. However, for the dicationic final state $2^1\Delta$ an influence of an avoided level crossing can be excluded, since it is the only state with this symmetry in the considered energy region. Consequently, we assume the predicted metastability to be valid.

The intensities of the transitions to the $2^1\Delta$ state, resulting from the present assignment, are much lower than the theoretical values discussed further below. This may question the given assignment, in particular since an alternative assignment for the transitions are Auger decays of S $2p^{-1}$ satellite lines, which are expected to be very weak.[8,47] However, such an assignment is even less convincing, since it would require the unlikely case that the following three prerequisites are fulfilled: First, the final states $1^1\Pi$ and $2^1\Delta$ are – contrary to expectation – both dissociative and overlap almost perfectly, since only this would explain that just one state is observed. Second, the S $2p^{-1}$ satellite line is stable with respect to dissociation and possesses a ligand-field splitting that deviates less than 20 meV from that of the S $2p^{-1}$ main component. Third, the geometry of the S $2p^{-1}$ satellite state matches that of the final state very well.

The peak at 133.61 eV in the S $2p_{3/2}^{-1}$ AES, reported by Bolognesi *et al.*,[13] is much narrower than the other peaks in their spectrum; it can be related to the S $2p_{3/2}^{-1} \rightarrow 2^3\Pi$ transition in the present spectrum. This assignment is based on an additional splitting of the transition as well as the intensity ratio of the subcomponents, see below. It is also in full agreement with the assignment of Eland,[6] who observed a line broadening and suggested that this is caused by a splitting of a triplet state.

In the energy region of the peak at 133.05 eV in the S $2p_{3/2}^{-1}$ AES of Bolognesi *et al.*,[13] the present high-resolution measurements reveal three different transitions. One of these Auger transitions shows broad lines, and the corresponding final state is labeled by "?" due its rather unclear nature, see below. The remaining two transitions consist of narrow lines so that we relate them to the expected Auger transitions in this energy region, namely S $2p_{3/2}^{-1} \rightarrow 2^1\Sigma^+$ and S $2p_{3/2}^{-1} \rightarrow 2^1\Pi$. However, neither the present experimental results alone nor a combination with the available theoretical results allow to give a conclusive assignment for these two transitions, in particular since this would also depend on the assignment of the transition to the final state labeled "?". In order to simplify the following discussion concerning these two Auger transitions, we will label the final state of the Auger transition at lower kinetic energy *A* and the one at higher kinetic energies *B*.

In the following, we will discuss two possible assignments of the final state labeled "?" and consider the consequences of these assignments. The first possible assignment is an Auger decay of a satellite excitation in the PES. Such contributions in the AES subsequent to $2p^{-1}$ ionization have been observed before for HCl (Ref. 8) and H_2S.[47] An assignment along these lines would be in agreement with the low intensity of the Auger transition, since such satellite lines are normally quite weak in the PES. State *A* can then be assigned to $2^1\Sigma^+$ and state *B* to $2^1\Pi$, since the theoretical results presented in Table IV give a higher Auger rate for the latter transition, in agreement with the experiment. As a consequence, the kinetic energy of Auger electrons related to $2^1\Sigma^+$ is by $\simeq$160 meV lower than that of $2^1\Pi$ and by $\simeq$750 meV lower than that of $2^3\Pi$. Contrary to this, the theoretical results in Table IV predict kinetic energies that are by -0.01 to 0.41 eV higher than those of $2^3\Pi$ and by 0.94–1.15 eV higher than of $2^1\Pi$. Therefore, the discussed assignment leads to a situation, where the

experimental kinetic energy of the Auger electrons related to the $2^1\Sigma^+$ state is – on a relative energy scale – by more than 1 eV lower than predicted by all calculations. The same effect, but with opposite sign, is observed for $2^3\Sigma^-$, see above. Both final states belong to the $2\pi^{-1}3\pi^{-1}$ configuration, with $2^3\Sigma^-$ [$2^1\Sigma^+$] being the one with the highest [lowest] kinetic energy. This might indicate that all calculations underestimate systematically the splitting between the states that belong to the $2\pi^{-1}3\pi^{-1}$ configuration.

The second possible assignment relates the final state "?" to higher vibrational substates of the Auger transition to A, however, with a considerable line broadening. Such a broadening effect for higher vibrational substates can be explained by a shallow potential minimum that can host only a small number of vibrational substates. In this case, the higher vibrational levels may have a shorter lifetime due to fast tunneling through the potential barrier or may even be continuum states; both situations would explain the broadening effect. Such an explanation would be in line with the observed energy splitting of $\simeq$300 meV between the state "?" and the state A as well as with the fact that the Auger transition to the state A consists of almost only the $v'' = (00) \rightarrow v' = (00)$ line. The suggested broadening effect has been observed before in the resonant Auger electron spectrum of HBr.[48] As a consequence of this assignment for the state "?", we have to take into account the sum intensity of the transitions to the states A and "?" for an assignment of the states A and B. However, the intensity ratio between the transitions to the states A plus "?" and transition to B is less pronounced than the ratio between transitions to A and B alone so that the above intensity arguments for a tentative assignment to the transitions S $2p_{3/2}^{-1} \rightarrow 2^1\Sigma^+$ and S $2p_{3/2}^{-1} \rightarrow 2^1\Pi$ no longer hold.

In summary, the assignment of transitions to the final states A, B, and "?" is rather unclear at the moment. However, additional more sophisticated calculations or further high-resolution photoelectron-Auger-electron coincidence spectra, as described by Ulrich *et al.*,[49] should allow to shed light on this part of the spectrum. In particular, coincidence spectra should allow to distinguish between the two possible assignments of the state "?".

2. Results of fit analysis

To extract information on the potential-energy surfaces of the metastable final states and the Auger intensities of the corresponding transitions, we performed a Franck-Condon analysis. However, three facts rendered it impossible to determine the vibrational energies of all states correctly. First, for some of the Auger transitions only the $v = (00)$ vibrational substate is clearly visible, while the higher vibrational substates are extremely weak. Second, the transitions are on a nonlinear background that is not exactly known. Third, the Auger transitions to the final states $2^3\Pi$ and B exhibit excitations of both the C−O and the C−S stretching vibrational modes. To overcome these problems, we reduced the number of free parameters by relating ΔQ_1 and $\hbar\omega_1$ of the C−O stretching vibrational mode to each other by using the approximation $R_e^2 \cdot \hbar\omega_1 = const$ for different electronic states of a given molecule,[50,51]

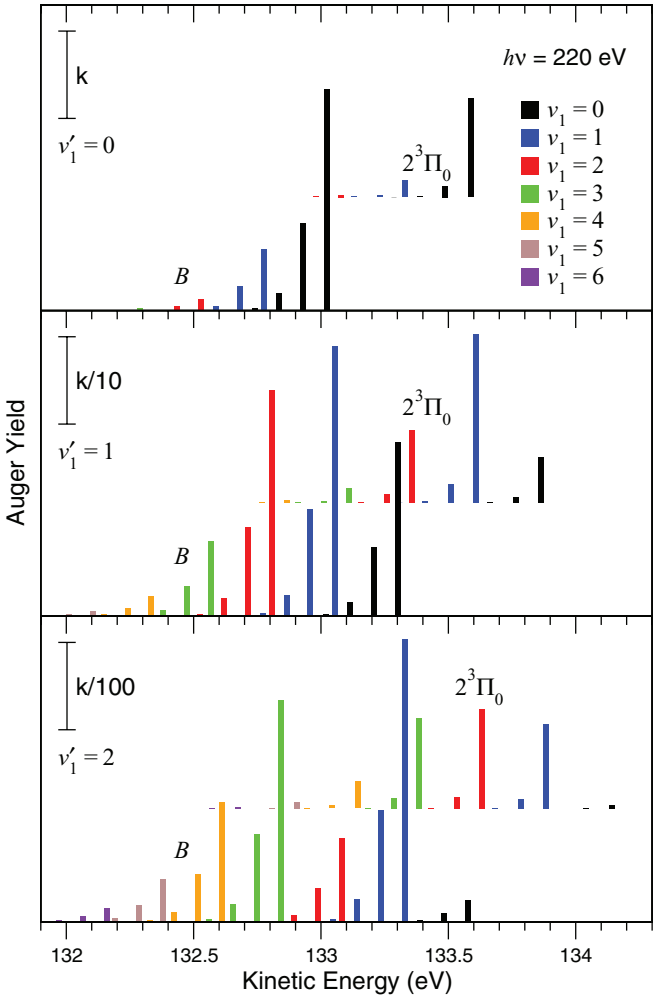

FIG. 6. Detailed vibrational structure of the S $2p_{1/2}^{-1} \rightarrow 2^3\Pi_0$ and S $2p_{1/2}^{-1} \rightarrow B$ Auger transitions as obtained from our fit analysis. Note that the intensity ratios of the frames with $v' = 0$, 1, and 2 are 100 : 10 : 1, respectively.

which was originally established for diatomic molecules. We tested this relation for the present case of OCS by applying it to R_e(C−O) and $\hbar\omega_1$ of the ground state, the S $2p^{-1}$ core-ionized state, and the dicationic final state $8\sigma^{-1}9\sigma^{-1}(^1\Sigma^+)$ (see below), which all have the same value of the normal coordinate Q_3, we found it to be valid within 5%. Therefore, we used these states to establish a relationship between R_e(C−O) and $\hbar\omega_1$, which was included in the fit analysis. By including also the C−S stretching vibrational mode for some of the transitions, we obtained an excellent fit result for this energy region, which is displayed in Fig. 5.

The Morse parameters extracted from the fit analysis of the transitions to the states $2^1\Delta$ and $2^3\Pi$ as well as those labeled A and B are also listed in Tables II and III. In addition, the detailed vibrational progression, including the C−O and the C−S vibrational mode of the transitions to the final states B and $2^3\Pi$, are shown in Fig. 6. A comparison of the equilibrium distances with the calculated results shows that the experimental values for the C−O and the C−S distances are on average by $\simeq$0.1 Å and $\simeq$0.15 Å, respectively, smaller than the theoretical values. In addition, the $2^3\Pi$ state is clearly stable with respect to dissociation, although the calculations

do not give a minimum along the C−S bond distance. However, this potential-energy surface is strongly influenced by an avoided level crossing with the $3^3\Pi$ state, and a slightly different potential-energy surface for the latter state could easily result in a metastable $2^3\Pi$ state. This means that the accuracy of a given potential-energy surface depends on the accuracy of all other potential-energy surfaces of states with the same symmetry. In general, the agreement between an experimentally determined and a calculated potential-energy surface is not very accurate in this energy region. This low accuracy is probably due to the fact that the geometries of the molecule are not fully optimized. Instead, the curves along the C−S distance are calculated with a fixed value for the C−O distance and vice versa.

In the fit analysis, it turned out that the centroids of the structures at ≃133.5, 133.6, and 134.7 eV, which are assigned to the $2^3\Pi$ state, do not fully obey the spin-orbit and the ligand-field splittings of the S $2p^{-1}$ core-ionized state; instead, they are shifted by some 10 meV. This finding suggests a spin-orbit splitting of the $2^3\Pi$ state into the components $2^3\Pi_2$, $2^3\Pi_1$, and $2^3\Pi_0$. Consequently, these three spectral features are fitted using three final states with an equidistant splitting. For the resulting nine transitions, we assumed the same vibrational progression, but different Auger intensities. In this way, we obtained a splitting of 22(1) meV between each two neighboring states, in full agreement with calculations by Hochlaf;[29] resulting in the $2^3\Pi_2$ state being the lowest in energy as well as a splitting of 21 meV between each two states. In Fig. 5, the Auger transition rates are indicated by vertical-bar diagrams and show a different behavior for the three components of the $2^3\Pi$ final state. In particular, the intensity of the S $2p^{-1}_{3/2,3/2} \rightarrow 2^3\Pi_0$ transition vanishes almost completely. This can readily be understood by selection rules if one takes the 100% π-character of the S $2p^{-1}_{3/2,3/2}$ core-hole state into account, i.e., the fact that it is a pure $^2\Pi_{3/2}$-state. For a transition to a $^3\Pi_0$ state, the outgoing Auger electron must have σ symmetry, and it has to carry an angular momentum Ω of 3/2, which is forbidden on the basis of angular-momentum arguments. These observations clearly support the given assignment for the discussed structures.

C. S $2p^{-1} \rightarrow 8\sigma^{-1}9\sigma^{-1}(^1\Sigma^+)$ Auger transitions

The energy region from 128.3 to 132 eV is shown in Fig. 7, including the fit result. From the experimental data points we clearly see a vibrational structure with a spacing of ≃240 meV, which is typical for the C−O stretching vibrational mode. In the fit analysis of this region, we found only one state with a vibrational structure. In addition, the S $2p^{-1}_{3/2,3/2}$ component of the corresponding Auger transition is missing. An assignment of this transition was achieved by using the results of our calculations presented in Table I and in the lower part of Fig. 2. In the discussed kinetic-energy region of the state indicated by *m*, the intensity of only the S $2p^{-1}_{3/2,3/2}$ component is calculated to be almost zero, while the two other components have much higher intensities. Therefore, we assign this transition to S $2p^{-1} \rightarrow 8\sigma^{-1}9\sigma^{-1}(^1\Sigma^+)$.

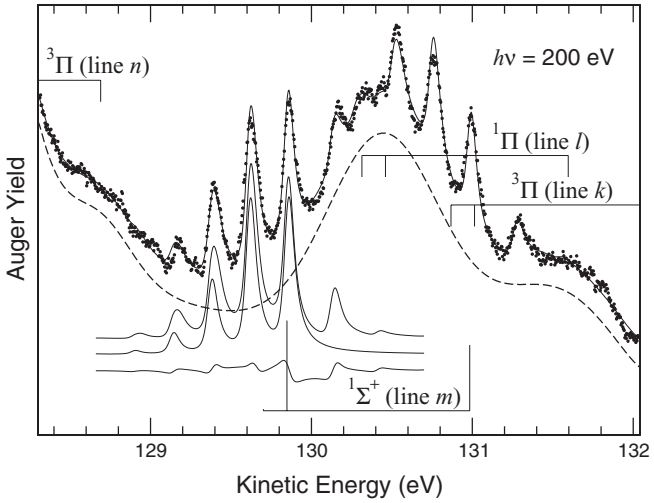

FIG. 7. Normal AES of the OCS molecule subsequent to S $2p^{-1}$ photoionization with 200-eV photons recorded in the kinetic-energy region from 128.3 to 132 eV. The solid line through the data points represents the fit result, and the dashed subspectrum the background that consists of transitions to dissociative final states. The vertical-bar diagram at the bottom indicates the intensities and energy positions of the $v' = (00) \rightarrow v = (00)$ transitions to the final state $8\sigma^{-1}9\sigma^{-1}(^1\Sigma^+)$, and the upper vertical-bar diagrams the approximate energy positions of all transitions to dissociative final states. The upper solid subspectrum indicates the vibrational progression of the S $2p_{3/2,\,1/2} \rightarrow 8\sigma^{-1}9\sigma^{-1}(^1\Sigma^+)$ Auger transition (line m). The middle (lower) solid subspectrum shows the contributions originating from the Auger decay of vibrational level $v' = (00)$ of the core-ionized state alone (the vibrational lifetime interference contribution).

The missing S $2p^{-1}_{3/2,3/2} \rightarrow 8\sigma^{-1}9\sigma^{-1}(^1\Sigma^+)$ component indicates clearly that the $2p\pi^{-1} \rightarrow 8\sigma^{-1}9\sigma^{-1}(^1\Sigma^+)$ Auger rate is very low, while the whole intensity is carried by the $2p\sigma^{-1} \rightarrow 8\sigma^{-1}9\sigma^{-1}(^1\Sigma^+)$ transition. This allows one to estimate the $2p\sigma^{-1}$ contributions of the S $2p^{-1}_{3/2,1/2}$ and the S $2p^{-1}_{1/2}$ core-hole states as 55% and 45%, respectively, by considering the intensity ratio of the corresponding Auger transitions. These values are in good agreement with the values of 57% for the S $2p^{-1}_{3/2,1/2}$ core-hole state and of 43% for the S $2p^{-1}_{1/2}$ core-hole state as calculated by Kosugi *et al.*[46] To our knowledge, this is the first direct experimental determination of the orientation of spin-orbit and ligand-field split $2p^{-1}$ core holes.

The results of the Franck-Condon analysis are also summarized in Tables II and III. However, since the $8\sigma^{-1}9\sigma^{-1}(^1\Sigma^+)$ state is more than 10 eV above the ground state of dicationic OCS, calculations of the potential-energy surfaces are not available for comparison.

The dashed subspectrum indicates the background employed in the fit analysis. It consists of broad spin-orbit split spectral features at ≃130.4 and ≃131.5 eV. We assign these features to S $2p^{-1} \rightarrow 2\pi^{-1}9\sigma^{-1}(^1\Pi)$ transitions (line *l*), since the ratio of their intensities and the intensities of the S $2p^{-1} \rightarrow 8\sigma^{-1}9\sigma^{-1}(^1\Sigma^+)$ transitions agree well with the present theoretical prediction. By taking into account that the present calculated energies of the lines *n* and *o* are clearly too high, see Fig. 2, we assign the broad spectral feature at ≃128.5 eV to the S $2p^{-1}_{1/2} \rightarrow 2\pi^{-1}9\sigma^{-1}3\pi^{-1}4\pi^1(^3\Pi)$ transition (line *n*), although its intensity is underestimated in the

TABLE V. Kinetic energies, E_{kin}, and branching ratios as obtained from intensities of the Auger transitions. The branching ratios are normalized to the intensity of the transition S $2p_{1/2}^{-1} \rightarrow \tilde{a}^1\Delta$. The listed branching ratios are mean values derived from the spectra recorded at photon energies of 220 and 240 eV. Kinetic energies are shown for the transitions between potential-energy minima of the S $2p_{1/2}^{-1}$ state and the presented dicationic states. Note that the error bars for the kinetic energies do not include an error of 0.06 eV for the calibration of the entire energy scale.

		Relative intensity$_{exp}$				Relative intensity$_{th}$				
State	Configuration	S $2p_{1/2}^{-1}$	S $2p_{3/2,1/2}^{-1}$	S $2p_{3/2,3/2}^{-1}$	$\sum$ 2p	S $2p_{1/2}^{-1}$	S $2p_{3/2,1/2}^{-1}$	S $2p_{3/2,3/2}^{-1}$	$\sum$ 2p	E_{kin}, eV
$\tilde{X}^3\Sigma^-$	$3\pi^{-2}$	0.646(5)	0.75(2)	1.02(3)	2.42(6)	0.958	0.731	1.689	3.378	
$\tilde{a}^1\Delta$	$3\pi^{-2}$	1	0.99(1)	2.02(5)	4.01(6)	1	0.785	1.695	3.480	140.87(1)
$\tilde{b}^1\Sigma^+$	$3\pi^{-2}$	0.626(1)	0.61(2)	1.19(4)	2.42(6)	0.537	0.421	0.914	1.872	139.89(1)
$2^1\Delta$	$2\pi^{-1}3\pi^{-1}$	0.012(7)	0.028(2)	0.0539(5)	0.09(1)	0.234	0.184	0.399	0.817	135.36(3)
$2^3\Pi_2$	$8\sigma^{-1}3\pi^{-1}$	0.053(7)	0.025(1)	0.173(2)	0.25(1)					134.77(1)
$2^3\Pi_1$	$8\sigma^{-1}3\pi^{-1}$	0.04(2)	0.06(2)	0.0580(4)	0.15(4)					134.75(1)
$2^3\Pi_0$	$8\sigma^{-1}3\pi^{-1}$	0.11(2)	0.09(1)	0.005(4)	0.20(4)					134.73(1)
$2^3\Pi$ sum	$8\sigma^{-1}3\pi^{-1}$	0.20(5)	0.18(3)	0.236(8)	0.61(9)	0.284	0.260	0.366	0.909	
$2^1\Pi$	$8\sigma^{-1}3\pi^{-1}$					0.336	0.307	0.429	1.073	
B		0.340(8)	0.226(5)	0.184(7)	0.75(2)					134.16(1)
$2^1\Sigma^+$	$2\pi^{-1}3\pi^{-1}$					0.141	0.111	0.239	0.491	
A		0.123(4)	0.108(4)	0.091(3)	0.32(1)					134.00(1)
$^1\Sigma^+$	$8\sigma^{-1}9\sigma^{-1}$	0.128(1)	0.163(3)	0.003(2)	0.294(7)	0.058	0.075	0.005	0.138	131.00(1)

present theoretical results; this can be seen clearly in Fig. 2. In this figure the S $2p_{3/2}^{-1}$ components of these Auger transitions exhibit high intensities between the lines at ≃126.8 and 128 eV, which are assigned to $9\sigma^{-2}(^1\Sigma^+)$ (line *o*). The intense line *n* is also clearly visible in the S $2p_{3/2}^{-1}$ AES presented by Bolognesi *et al.*[13]

In addition, the present calculations, as well as those of Minelli *et al.*,[15] predict that the Auger transitions to the final state $2\pi^{-1}9\sigma^{-1}(^3\Pi)$ (line k) have non-vanishing intensities. Moreover, the kinetic energies of the Auger electrons related to transitions to this final state are calculated to be higher by 0.7–1.0 eV as compared to those of the transition to the final state $8\sigma^{-1}9\sigma^{-1}(^1\Sigma^+)$, with the consequence that the S $2p_{3/2}^{-1}$ components are located at 131 eV. This assignment is in agreement with double charge-transfer measurements of Langford *et al.*,[52] who also observed a triplet state ∼9 eV above the ground state of OCS^{2+}. Moreover, this assignment also explains the weak spectral feature at 132.2 eV as S $2p_{1/2}^{-1} \rightarrow 3^3\Pi$, see Fig. 5.

D. Experimental and theoretical Auger intensities

Table V summarizes the present experimental and theoretical intensities of the observed Auger transitions. The values for the various core holes as well as the total S $2p^{-1}$ Auger intensities to the individual metastable final states are given. All these values are normalized to the S $2p^{-1} \rightarrow \tilde{a}^1\Delta$ Auger transition. For the clearly assigned states, the experimental and theoretical total S $2p^{-1}$ Auger intensities agree on a qualitative level, with the exception of the Auger transitions to the $2^1\Delta$ final state. In this case, the theoretical Auger intensities are approximately by one order of magnitude too large; this will be discussed further below.

The experimental Auger intensities vary significantly for the different core holes. In particular, the intensities of the Auger transitions from the S $2p_{1/2}^{-1}$ and S $2p_{3/2,1/2}^{-1}$ core holes to the final states $\tilde{X}^3\Sigma^-$, $\tilde{a}^1\Delta$, $\tilde{b}^1\Sigma^+$, $2^1\Delta$, and $2^3\Pi$ are lower than those starting from the S $2p_{3/2,3/2}^{-1}$ core hole. Contrary to this, the S $2p_{3/2,3/2}^{-1}$ component of the Auger transition to the final state $8\sigma^{-1}9\sigma^{-1}(^1\Sigma^+)$ vanishes almost completely. All these findings are qualitatively reproduced by the calculations and can be explained on the basis of the orientation of the core hole relative to the valence orbitals from which the electrons are missing.[44,45] On a more detailed level, it turned out that for the states $\tilde{X}^3\Sigma^-$, $\tilde{a}^1\Delta$, $\tilde{b}^1\Sigma^+$, and $2^3\Pi$, the intensities of the S $2p_{3/2,3/2}^{-1}$ Auger transitions are overestimated by theory. Moreover, the theoretical intensities of the S $2p_{3/2,1/2}^{-1}$ Auger transitions to the final states $\tilde{X}^3\Sigma^-$, $\tilde{a}^1\Delta$, and $\tilde{b}^1\Sigma^+$ are lower than those of the S $2p_{1/2}^{-1}$ Auger transitions; in contrast to this, the experimental intensities are almost identical. All these observations are in line with the fact that the present theory overestimates the total $2p\pi^{-1}$ Auger rates as compared to the total $2p\sigma^{-1}$ Auger rates; see discussion about lifetime broadening in Sec. IV.

VI. SUMMARY AND CONCLUSIONS

In the present work, the S $2p^{-1}$ PES and the spectrum of the subsequent Auger decays are presented at high energy resolution. For the vibrationally resolved PES, a Franck-Condon analysis was performed and information on the potential-energy surface was derived. In addition, the lifetime broadenings of the individual core-hole states were obtained.

In the AES, transitions to eight metastable final states were observed. In addition, we present calculations on the Auger intensities, which take the core-hole orientation of the different spin-orbit and ligand-field split S $2p$ levels into account. Using the results of these calculations, in combination with previous results available in the literature, and an experimentally observed splitting that clearly identified one final state as $2^3\Pi$, we were able to assign six of the observed metastable final states. The remaining two final states are

related to the final states $2^1\Sigma^+$ and $2^1\Pi$. We also present an assignment for transitions to dissociative states.

Auger transitions to seven of the metastable final states exhibit excitations of the C−O stretching vibrational mode and partially also of the C−S stretching vibrational mode. This allowed us to perform a Franck-Condon analysis of the transitions and to derive information on the potential-energy surfaces of the corresponding dicationic final states. Up to now, the experimentally obtained potential-energy surfaces are reproduced well by theory for only two of the final states, namely $\tilde{a}^1\Delta$ and $\tilde{b}^1\Sigma^+$, which both belong to the ground-state configuration $3\pi^{-2}$.

The Auger transition to the ground state $\tilde{X}^3\Sigma^-$ of OCS^{2+} exhibits only weak vibrational structures, which originate from the C−S stretching vibrational mode, and it turned out that a description within the Franck-Condon approximation is not possible. We assume that this state possesses a complicated vibrational structure with contributions of the bending vibrational mode, which might be due to Fano resonances.

For the S $2p^{-1} \rightarrow 8\sigma^{-1}9\sigma^{-1}(^1\Sigma^+)$ transition, the S $2p^{-1}_{3/2,3/2}$ component is missing. This peculiarity allowed an unambiguous assignment of this transition. Since this core hole has a pure S $2p\pi^{-1}$ orientation, we were able to derive the core-hole orientation for the three spin-orbit and ligand-field split S $2p^{-1}$ states; the obtained results are in good agreement with theoretical predictions.

A comparison of the present theoretical results with the experimental findings, in general shows good agreement, with a few exceptions. First, the kinetic energies of the transitions to the $2^3\Sigma^-$ state are too low and those of the transitions to the $2^1\Sigma^+$ state are too high by ∼1 eV each. On this point, the present calculations agree well with those presented in Refs. 5 and 15. Second, the theoretical relative Auger intensities of the S $2p^{-1} \rightarrow 2^1\Delta$ transition are by approximately one order of magnitude too large. Interestingly, all final states belong to the $2\pi^{-1}3\pi^{-1}$ configuration. This suggests that calculations concerning this configuration are difficult to perform and require special attention. Third, the calculated intensities of the $2p\sigma^{-1}$ Auger decays are underestimated as compared to those of the $2p\pi^{-1}$ Auger decays. This explains most of the differences between the experimental and theoretical branching ratios of the spin-orbit and ligand-field split Auger transitions.

In summary, a considerably improved understanding of the S $2p^{-1}$ AES of OCS and the corresponding dicationic final states has been achieved. For further improvement, more accurate calculations of the potential-energy surfaces and of the vibrational structures are required. This holds in particular for the ground state $\tilde{X}^3\Sigma^-$ of OCS^{2+} as well as for all states that do not belong to the $3\pi^{-2}$ configuration. Additional experimental studies are also required. For example, high-resolution photoelectron-Auger-electron coincidence studies would allow to separate the overlapping AES that originate from the different spin-orbit and ligand-field split core holes. Such studies would in particular allow to separate the strongly overlapping Auger transitions to dissociative parts of the potential-energy surfaces and to derive their individual Auger intensities. They would also allow to identify possible contributions of Auger transitions originating from S $2p^{-1}$ satellite lines.

When comparing the typical lifetime broadenings of 90 meV and 150 meV for the C $1s^{-1}$ and O $1s^{-1}$ core-hole states, respectively, with the vibrational energies of about 250 meV for the C-O stretching mode, we expect to be able to resolve vibrational structures in the corresponding spectra. It would therefore be interesting to record also complimentary high-resolution C $1s^{-1}$ and O $1s^{-1}$ AES, since in these cases partly different final states will populated.[12,15] In addition, the C $1s^{-1}$ and O $1s^{-1}$ core-hole states of OCS have different geometries, which means that different parts of the potential-energy surfaces of the diatomic final states are probed by the two Auger processes.

ACKNOWLEDGMENTS

This work was supported by the Deutsche Forschungsgemeinschaft, Project No. Pu 180/6-1, and by the Research Council for Natural Sciences of the Academy of Finland. R.P. gratefully acknowledges fruitful discussions with Professor Majdi Hochschlaf. We also acknowledge experimental support and technical assistance by Virpi Pennanen and Marko Jurvansuu as well as by the staff of Maxlab.

[1] L. Leman, L. Orgel, and M. R. Ghadiri, Science **306**, 283 (2004).
[2] A. S. Newton, J. Chem. Phys. **40**, 607 (1964).
[3] J. D. H. Eland, M. Hochlaf, P. Linusson, E. Andersson, L. Hedin, and R. Feifel, J. Chem. Phys. **132**, 014311 (2010).
[4] J. Ridard, B. Levy, and P. Millié, Chem. Phys. **122**, 403 (1988).
[5] V. Brites, J. H. D. Eland, and M. Hochlaf, Chem. Phys. **346**, 23 (2008).
[6] J. H. D. Eland, Chem. Phys. **294**, 171 (2003).
[7] R. Püttner, Y. F. Hu, G. M. Bancroft, H. Aksela, E. Nõmmiste, J. Karvonen, A. Kivimäki, and S. Aksela, Phys. Rev. A **59**, 4438 (1999).
[8] R. Püttner, V. Pennanen, T. Matila, A. Kivimäki, M. Jurvansuu, H. Aksela, and S. Aksela, Phys. Rev. A **65**, 042505 (2002).
[9] R. Püttner, X.-J. Liu, H. Fukuzawa, T. Tanaka, M. Hoshino, H. Tanaka, J. Harries, Y. Tamenori, V. Carravetta, and K. Ueda, Chem. Phys. Lett. **445**, 6 (2007).
[10] A. Cesar, H. Ågren, and V. Carravetta, Phys. Rev. A **40**, 187 (1989).
[11] F. Duschinsky, Acta Physicochim. **7**, 551 (1937).
[12] T. X. Carroll, De Ji, and T. D. Thomas, J. Electron Spectrosc. Relat. Phenom. **51**, 471 (1990).
[13] P. Bolognesi, P. O'Keeffe, and L. Avaldi, J. Phys. Chem. A **113**, 15136 (2009).
[14] T. Kaneyasu, M. Ito, Y. Hikosaka, and E. Shigemasa, J. Korean Phys. Soc. **54**, 371 (2009).
[15] D. Minelli, F. Tarantelli, A. Sgamellotti, and L. S. Cederbaum, J. Chem. Phys. **107**, 6070 (1997).
[16] S. Masuda, T. Hatsui, and N. Kosugi, J. Electron Spectrosc. Relat. Phenom. **137–140**, 351 (2004).
[17] I. Nenner, M. Hubin-Franskin, J. Delwiche, P. Morin, and S. Bodeur, J. Mol. Struct. **173**, 269 (1988).
[18] R. F. Fink, A. Eschner, M. Magnuson, O. Björneholm, I. Hjelte, C. Miron, M. Bässler, S. Svensson, M. N. Piancastelli, and S. L. Sorensen, J. Phys. B **39**, L269 (2006).
[19] M. Magnuson, J. Guo, C. Såthe, J.-E. Rubensson, J. Nordgren, P. Glans, L. Yang, P. Salek, and H. Ågren, Phys. Rev. A **59**, 4281 (1999).
[20] T. R. Walsh, T. E. Meehan, and F. P. Larkins, J. Phys. B **29**, 207 (1996).
[21] M. Bässler, A. Ausmees, M. Jurvansuu, R. Feifel, J.-O. Forsell, P. de Tarso Fonseca, A. Kivimäki, S. Sundin, S. L. Sorensen, R. Nyholm, O. Björneholm, S. Aksela, and S. Svensson, Nucl. Instrum. Methods Phys. Res. A **469**, 382 (2001).
[22] M. Coville and T. D. Thomas, J. Electron Spectrosc. Relat. Phenom. **71**, 21 (1995).
[23] N. Correia, A. Flores-Riveros, H. Ågren, K. Helenelund, L. Asplund, and U. Gelius, J. Chem. Phys. **83**, 2035 (1985).
[24] M. Halmann and I. Laulicht, J. Chem. Phys. **43**, 438 (1965).
[25] H. A. Ory, A. P. Gittelman, and J. P. Maddox, Astrophys. J. **139**, 346 (1964).

[26]Gmelin Handbuch der Anorganischen Chemie, Kohlenstoff Teil D 5, System-Nummer 14, (Springer-Verlag, 1977).
[27]L. C. Cederbaum and W. Domcke, J. Chem. Phys. **64**, 603 (1976).
[28]N. B. Colthup, L. H. Daly, and S. E. Wiberley, *Introduction to Infrared and Raman Spectroscopy* (Academic, 1990).
[29]M. Hochlaf, private communication (2010).
[30]M. Yu. Kuchiev and S. A. Sheinerman, Zh. Eksp. Teor. Fiz. **90**, 1680 (1986) [Sov. Phys. JETP **63**, 986 (1986)].
[31]G. B. Armen, J. Tulkki, T. Åberg, and B. Crasemann, Phys. Rev. A **36**, 5606 (1987).
[32]R. Püttner, V. Sekushin, G. Kaindl, X.-J. Liu, H. Fukuzawa, K. Ueda, T. Tanaka, M. Hoshino, and H. Tanaka, J. Phys. B **41**, 045103 (2008).
[33]H. Siegbahn, L. Asplund, and P. Kelfve, Chem. Phys. Lett. **35**, 330 (1975).
[34]H. Ågren, S. Svensson, and U. Wahlgren, Chem. Phys. Lett. **35**, 336 (1975).
[35]R. Fink, J. Electron Spectrosc. Relat. Phenom. **76**, 295 (1995).
[36]R. F. Fink, M. Kivilompolo, H. Aksela, and S. Aksela, Phys. Rev. A **58**, 1988 (1998).
[37]T. H. Dunning, Jr., J. Chem. Phys. **90**, 1007 (1989).
[38]R. F. Fink, S. L. Sorensen, A. Naves de Brito, A. Ausmees, and S. Svensson, J. Chem. Phys. **112**, 6666 (2000).
[39]M. H. Chen, F. P. Larkins, and B. Crasemann, At. Data Nucl. Data Tables **45**, 1 (1990).
[40]K. J. Børve, Chem. Phys. Lett. **262**, 801 (1996).
[41]See supplementary material at http://dx.doi.org/10.1063/1.4734310 for a complete list of the calculated electronic states corresponding to Table I.
[42]M. R. F. Siggel, C. Field, L. J. Sæthre, K. J. Børve, and T. D. Thomas, J. Chem. Phys. **105**, 20 (1996).
[43]E. Kukk, J. D. Bozek, J. A. Sheehy, P. W. Langhoff, and N. Berrah, J. Phys. B **33**, L51 (2000).
[44]A. M. Bueno, A. N. de Brito, R. F. Fink, M. Bässler, O. Björneholm, F. Burmeister, R. Feifel, C. Miron, S. L. Sorensen, H. Wang, and S. Svensson, Phys. Rev. A **67**, 022714 (2003).
[45]S. Svensson, A. Ausmees, S. J. Osborne, G. Bray, F. Gel'mukhanov, H. Ågren, A. Naves de Brito, O.-P. Sairanen, A. Kivimäki, E. Nõmmiste, H. Aksela, and S. Aksela, Phys. Rev. Lett. **72**, 3021 (1994).
[46]N. Kosugi and T. Ishida, Chem. Phys. Lett. **329**, 138 (2000).
[47]M. Poygin, R. Püttner, M. Martins, V. Pennanen, M. Jurvansuu, Y. H. Jiang, H. Aksela, S. Aksela, and G. Kaindl, Phys. Rev. A **74**, 012711 (2006).
[48]R. Püttner, Y. F. Hu, G. M. Bancroft, A. Kivimäki, M. Jurvansuu, H. Aksela, and S. Aksela, Phys. Rev. A **77**, 032705 (2008).
[49]V. Ulrich, S. Barth, T. Lischke, S. Joshi, T. Arion, M. Mucke, M. Förstel, A. M. Bradshaw, and U. Hergenhahn, J. Electron Spectrosc. Relat. Phenom. **183**, 70 (2011).
[50]R. T. Birge, Phys. Rev. **25**, 240 (1925).
[51]R. Mecke, Z. Phys. **32**, 823 (1925).
[52]M. L. Langford, F. M. Harris, C. J. Reid, J. A. Ballantine, and D. E. Parry, Chem. Phys. **149**, 455 (1991).